J. Am. Chem. Soc. **1990**, *112*, 7462–7474

Studies of the Solution Structure of the Bleomycin A_2–Iron(II)–Carbon Monoxide Complex by Means of Two-Dimensional NMR Spectroscopy and Distance Geometry Calculations

Marcel A. J. Akkerman,[†] Eric W. J. F. Neijman,[†] Sybren S. Wijmenga,[†] Cornelis W. Hilbers,*[,†] and Wolfgang Bermel[‡]

Contribution from the Department of Biophysical Chemistry, Faculty of Science, University of Nijmegen, Toernooiveld, 6525 ED Nijmegen, The Netherlands, and Bruker Analytische Messtechnik GmbH, Silberstreifen, D-7512 Rheinstetten, West Germany. *Received May 1, 1989*

Abstract: As part of our program to delineate the solution structure of bleomycin–metal complexes and the DNA complexes thereof, we studied the bleomycin–iron(II)–carbon monoxide complex. With aid of various 2D NMR techniques we were able to assign the ^1H and ^{13}C NMR spectra of this complex completely. Vicinal coupling constant analysis, ^{13}C chemical shift information, and NOE data revealed the active participation of five iron binding sites in the bleomycin molecule, namely, the secondary amine function of the β-aminoalanine fragment, the aromatic pyrimidine, the amide and imidazole group of the β-hydroxyhistidine residue, and the carbamoyl group of the mannose sugar. A study of the ^{13}C NMR spectrum of the corresponding enriched iron-57 complex enabled us to establish the carbon monoxide as the sixth iron binding site via a 30-Hz coupling constant between iron-57 and the carbon monoxide carbon-13 atom. Subsequently, NOE data and the five iron coordination sites in the bleomycin molecule were used as interpoint distances in distance geometry calculations. In this way, several acceptable structures were generated that represent the first three-dimensional structure of the bleomycin–iron(II)–carbon monoxide complex in solution. Also, a discussion is presented of some aspects of the structure–activity relationship.

Introduction

Bleomycin A_2 (BLM, Figure 1) belongs to a family of antitumor metalloglycopeptides produced by strains of *Streptomyces verticillus*. It was first isolated in 1966 as a copper(II) complex;[1,2] however, the iron(II)–oxygen adduct has been proposed as the biologically active species[3-7] and is believed to be responsible for the cellular degradation of DNA.[8] The iron–oxygen center produces reactive oxygen radicals, which mediate oxidative damage to DNA. The C4′ hydrogen of the deoxyribose moiety of a pyrimidine nucleotide adjacent to guanosine has been proposed as the site of action of these radicals.[6,7,9,10] The bithiazole fragment and perhaps the positively charged tail of BLM are required for DNA binding and sequence-specific recognition.[11,12]

As part of our program to delineate the solution structure of bleomycin–metal compounds and the DNA adducts thereof, we studied the bleomycin–iron(II)–carbon monoxide (BLM–Fe–CO) complex. This complex is generally considered as a model for the putative active iron–oxygen complex. The iron coordination in the BLM–Fe–CO complex has been the subject of earlier studies. Takita et al.[13] proposed a structure for this complex in which both amine functions, the pyrimidine and imidazole groups, the histidine amide, and the carbon monoxide molecule are chelated to the iron(II) ion. This structure proposal was mainly based on the crystal structure of the copper(II) complex of P-3A,[14] a biosynthetic precursor of bleomycin. In contrast, the group of Oppenheimer[15] suggested, on the basis of the proton chemical shifts of the BLM–Fe–CO complex compared to those of the metal-free bleomycin, that, instead of the histidine amide, the mannose carbamoyl group is coordinated to the iron ion. In the present paper, a complete assignment is given of the ^1H and ^{13}C NMR spectra of the BLM–Fe–CO complex at pH 7. Furthermore, an assessment of the metal coordination sites is presented along with a discussion of the solution structure of this complex as compared to the structures of the metal-free bleomycin[16] and the bleomycin–zinc (BLM–Zn) molecule.[17,18]

Materials and Methods

Materials. Bleomycin A_2 sulfate was purchased from Nipponkayaku Co. (Tokyo, Japan). Samples were prepared under anaerobic (N_2) conditions. A 3-mg sample of bleomycin A_2 sulfate was lyophilized three times from 99.8% D_2O and dissolved in 300 μL of 99.95% D_2O. Subsequently, 10 μL of a 20 mM sodium dithionite solution in D_2O and 10 μL of a 0.195 M solution of $FeSO_4 \cdot 7H_2O$ in D_2O were added. The iron(II) sulfate was liberated from crystal water by heating and then dissolved in D_2O. Next, the pH was adjusted to 7 with 30 μL of a 0.1 M NaOD solution in D_2O, whereby the color of the solution changed from colorless to light pink. Finally, the sample was exposed to carbon monoxide gas (Hoek-Loos), causing the color of the solution to change to bright yellow. The samples were stored under a carbon monoxide atmosphere in sealed NMR tubes (Wilmad, 5-mm diameter). They could be kept at 277 K for several weeks without any noticeable disintegration. The final bleomycin concentration amounted to 5.4 mM. Samples prepared in H_2O solutions contained 5% D_2O.

[†] University of Nijmegen.
[‡] Bruker Analytische Messtechnik GmbH.

(1) Umezawa, H.; Maeda, K.; Takeuchi, T.; Okami, I. *J. Antibiot.* **1966**, *19*, 200.
(2) Umezawa, H.; Suhara, Y.; Takita, T.; Maeda, K. *J. Antibiot.* **1966**, *19*, 210.
(3) Sausville, E. A.; Peisach, J.; Horwitz, S. B. *Biochemistry* **1978**, *17*, 2740.
(4) Sausville, E. A.; Stein, R. W.; Peisach, J.; Horwitz, S. B. *Biochemistry* **1978**, *17*, 2746.
(5) Burger, R. M.; Berkowtiz, A. E.; Peisach, J.; Horwitz, S. B. *J. Biol. Chem.* **1980**, *255*, 11832.
(6) Giloni, L.; Takeshita, M.; Johnson, F.; Iden, C.; Grollman, A. P. *J. Biol. Chem.* **1981**, *256*, 8608.
(7) Wu, J. C.; Kozarich, J. W.; Stubbe, J. *J. Biol. Chem.* **1983**, *258*, 4694.
(8) Umezawa, H. In *Bleomycin: Current Status and New Developments*; Carter, S. K., Crooke, S. T., Umezawa, H., Eds.; Academic Press: New York, 1978; p 15.
(9) Wu, J. C.; Kozarich, J. W.; Stubbe, J. *Biochemistry* **1985**, *24*, 7562.
(10) Rabow, L.; Stubbe, J.; Kozarich, J. W.; Gerlt, J. A. *J. Am. Chem. Soc.* **1986**, *108*, 7130.
(11) Kross, J.; Henner, D.; Haseltine, W. A.; Rodriguez, L.; Levin, M. D.; Hecht, S. M. *Biochemistry* **1982**, *21*, 3711.
(12) Fisher, L. M.; Kuroda, R.; Sakai, T. *Biochemistry* **1985**, *24*, 3199.
(13) Takita, T.; Muraoka, Y.; Nakatani, T.; Fuji, A.; Iitaka, Y.; Umezawa, H. *J. Antibiot.* **1978**, *31*, 1073.
(14) Iitaka, Y.; Nakamura, H.; Nakatani, T.; Muraoka, Y.; Fujii, A.; Takita, T.; Umezawa, H. *J. Antibiot.* **1978**, *31*, 1070.
(15) Oppenheimer, N. J.; Rodriguez, L. O.; Hecht, S. M. *Proc. Natl. Acad. Sci. U.S.A.* **1979**, *76*, 5616.
(16) Haasnoot, C. A. G.; Pandit, U. K.; Kruk, C.; Hilbers, C. W. *J. Biomol. Struct. Dyn.* **1984**, *2*, 449.
(17) Akkerman, M. A. J.; Haasnoot, C. A. G.; Hilbers, C. W. *Eur. J. Biochem.* **1988**, *173*, 211.
(18) Akkerman, M. A. J.; Haasnoot, C. A. G.; Pandit, U. K.; Hilbers, C. W. *Magn. Reson. Chem.* **1988**, *26*, 793.

0002-7863/90/1512-7462$02.50/0

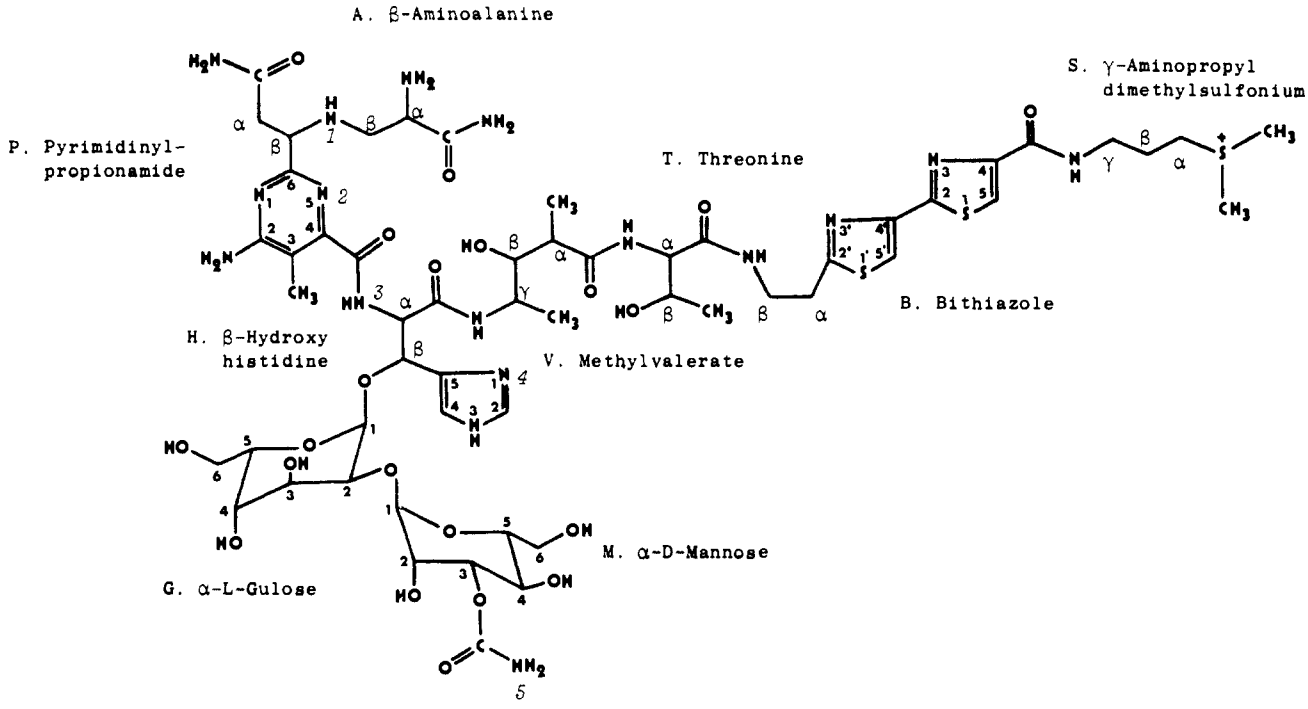

Figure 1. Structure of bleomycin A_2. Fragment abbreviations correspond to those in Table I. The numbers in boldface are referred to in the text. The numbering of the metal binding sites in Figure 14 correspond with the italic numbering in this figure.

The BLM-^{57}Fe-CO complex was prepared, with $^{57}FeCl_2$ as the iron source. The sample preparation was analogous to the method described above. $^{57}FeCl_2$ was synthesized from 95% enriched ^{57}Fe (Matheson) according to the literature.[19] A 34 mM sample of this complex was prepared in 1.3 mL of 99.95% D_2O solution. It was stored under a carbon monoxide atmosphere in a sealed NMR tube (Wilmad, 10-mm diameter) and could also be kept at 277 K for several weeks without any noticeable disintegration.

NMR Spectra. The ^{1}H NMR spectra were recorded on a Bruker AM 500 NMR spectrometer interfaced to an Aspect 3000 computer. Decoupling power is referenced in dB attenuation relative to a maximum of 20 W. The solvent (HDO or H_2O) signal was used as an internal reference (δ = 4.76 ppm at 300 K; δ = 4.97 ppm at 277 K) in the ^{1}H spectra. The ^{13}C 1D NMR spectra were recorded on a Bruker WM 200 NMR spectrometer, interfaced to an Aspect 2000 computer, using broad-band decoupling (11 dB of 20 W). The ^{1}H-^{13}C correlated 2D experiments were performed on a Bruker AM 600 NMR spectrometer (Bruker, Rheinstetten, West Germany). The methanol signal was used as an external reference (δ = 49.3 ppm at 300 K) in the ^{13}C spectra. The following 2D NMR methods were employed for the spectral assignments discussed in this paper.

Spin-Echo Correlated Spectroscopy (SECSY).[20,21] The experiment was performed at 277 K in D_2O. Prior to the standard SECSY pulse sequence, during the relaxation delay (rd) period (0.8 s), the HDO resonance was selectively irradiated (30 dB), resulting in the following pulse scheme:

$$[\mathrm{rd} - 90° - \tfrac{1}{2}t_1 - 90° - \tfrac{1}{2}t_1 - t_2]$$

Quadrature detection was used in both directions. For each value of t_1, 112 FIDs (2K data points, acquisition time 0.2048 s) were acquired. The value of t_1 was varied between 0.2 and 102.6 ms in steps of 200 μs. Prior to Fourier transformation, the FIDs were multiplied with a sine-bell window function in both directions. Spectra were calculated in absolute value mode.

Double-Quantum-Filtered COSY (DQFC).[22,23] The experiment was performed at 277 K on a H_2O solution. Prior to the DQFC pulse sequence, during the relaxation delay period, the H_2O solvent signal was selectively irradiated (1 s, 13 dB):

$$[\mathrm{rd} - 90° - t_1 - 90° - \mathrm{d1} - 90° - t_2]$$

Quadrature detection in the t_1 direction was achieved by using the TPPI method.[24] For each value of t_1, 80 FIDs were accumulated (2K data points, acquisition time 0.2048 s). The value of t_1 was varied over 0.003-51.203 ms in steps of 100 μs. The multiple-quantum evolution period (d1) amounted to 0.003 ms. Prior to Fourier transformation, the FIDs were multiplied with a sine-bell window function in both directions.

Nuclear Overhauser Enhancement Spectroscopy (NOESY) in D_2O.[25,26] The experiment was performed at 277 K. Quadrature detection in the t_1 direction was achieved by using the TPPI method.[24] During the relaxation delay period the HDO solvent signal was selectively irradiated (0.8 s, 30 dB):

$$[\mathrm{rd} - 90° - t_1 - 90° - t_m - 90° - t_2]$$

The spectra were recorded with a 400-ms mixing time (t_m). The value of t_1 was varied over 0.003-51.203 ms in steps of 100 μs. For each value of t_1, 80 FIDs were acquired (2K data points, acquisition time 0.2048 s). Prior to Fourier transformation, the FIDs were multiplied with Gauss-Lorentz-like window functions in both directions. Subsequently, the spectrum was submitted to a base-plane flattening procedure using the baseline correction algorithm of Pearson.[27]

Nuclear Overhauser Enhancement Spectroscopy (NOESY) in H_2O.[25,26] The experiment was performed at 277 K. In order to suppress the H_2O solvent signal, a time-shared long (TSL) observation pulse was used in combination with a data shift accumulation (DSA-4),[28,29] resulting in the following pulse sequence:

$$[\mathrm{rd} - 90° - \mathrm{d1} - t_1 - 90° - t_m - \mathrm{TSL\ pulse} - t_2]$$

Single side-band detection was used in the ω_1 direction (carrier frequency at low-field side of spectrum). A relaxation delay of 0.8 s was used. Prior to t_1, an extra delay (d1) of 25 μs was used for better water suppression. The total mixing time (t_m) of 400 ms included a homospoiling pulse of 50-ms duration.[30] The TSL pulse consisted of 10 9° pulses with intermittent delays of 39.0 μs. The value of t_1 was varied between 0.025 and 51.225 ms in steps of 100 μs. For each value of t_1, 96 FIDs were accumulated (4K data points, acquisition time 0.2048 s). Prior to Fourier

(19) *Inorganic Synthesis*; Jolly, W. L., Ed.; McCraw-Hill Book Co.: New York, 1939; p 102.
(20) Nagayama, K.; Wuethrich, K.; Ernst, R. R. *Biochem. Biophys. Res. Commun.* **1979**, *90*, 305.
(21) Nagayama, K.; Kumar, A.; Wuethrich, K.; Ernst, R. R. *J. Magn. Reson.* **1980**, *40*, 321.
(22) Shaka, A. J.; Freeman, R. *J. Magn. Reson.* **1983**, *51*, 169.
(23) Bax, A.; Edwards, M. W. *J. Am. Chem. Soc.* **1986**, *108*, 918.
(24) Marion, D.; Wuethrich, K. *Biochem. Biophys. Res. Commun.* **1983**, *113*, 967.
(25) Jeener, J.; Meier, B. M.; Bachmann, P.; Ernst, R. R. *J. Chem. Phys.* **1979**, *71*, 4546.
(26) Macura, S.; Ernst, R. R. *Mol. Phys.* **1980**, *41*, 95.
(27) Pearson, G. A. *J. Magn. Reson.* **1977**, *27*, 265.
(28) Haasnoot, C. A. G.; Hilbers, C. W. *Biopolymers* **1983**, *22*, 1259.
(29) Roth, K.; Kimber, B. J.; Feeney, J. *J. Magn. Reson.* **1980**, *41*, 302.
(30) Bax, A.; Mehlkopf, A. F.; Schmidt, J.; Freeman, R. *J. Magn. Reson.* **1980**, *41*, 502.

transformation, the FIDs were multiplied with a Gauss–Lorentz window function in both directions. Spectra were calculated in absorption mode[31] and subsequently submitted to a base-plane flattening procedure using a baseline correction algorithm of Pearson.[27]

^{1}H-Detected One-Bond ^{13}C–^{1}H Correlated Spectroscopy.[32,33] The experiment was performed at 298 K in D_2O using TPPI.[24] The following pulse sequence was used:

$$^1\text{H: } rd - 90° - \Delta - 180° - \Delta - 90° - \tfrac{1}{2}t_1 - 180° - \tfrac{1}{2}t_1 - \quad - t_2$$

$$^{13}\text{C: } rd - \quad - 180° - \quad - 90° - \quad - 90° -$$

During the relaxation delay period, the HDO solvent signal was selectively irradiated (1s, 30 dB relative to 20 W). The value of Δ amounted to 1.666 ms ($1/(4^1J_{CH})$). For each value of t_1, 56 FIDs were accumulated (2K data points, acquisition time 0.1617 s). The value of t_1 was varied over 0.003–16.998 ms in steps of 16.6 μs. Prior to Fourier transformation, the FIDs were multiplied with Gauss–Lorentz-like window functions in both directions.

^{1}H-Detected Multiple-Bond ^{13}C–^{1}H Correlated Spectroscopy.[34] The experiment was performed at 298 K in D_2O. A relaxation delay period of 1s was applied prior to the following pulse sequence:

$$^1\text{H: } rd - 90° - \Delta_1 - \quad - \tfrac{1}{2}t_1 - 180° - \tfrac{1}{2}t_1 - \quad - t_2$$

$$^{13}\text{C: } rd - \quad - 90° - \Delta_2 - 90° - \quad - 90° -$$

The value of Δ_1 ($1/(2^1J_{CH})$) amounted to 3.4 ms. In principle, the optimum choice of Δ_2 is $1/(2^nJ_{CH})$, where $^nJ_{CH}$ is the long-range coupling constant of interest. However, in practice, a somewhat shorter value (80 ms) is found to be optimal because decay of the ^{1}H magnetization occurs due to transverse relaxation and unresolved homonuclear couplings. For each value of t_1, 96 FIDs were acquired (2K data points, acquisition time 0.1716 s). The value of t_1 was varied over 0.003–32.768 ms in steps of 32 μs. Prior to Fourier transformation, the FIDs were multiplied with a sine-bell window function in the ω_2 direction. No digital filtering was applied in the ω_1 direction.

Distance Geometry Calculations.[35] The calculations were performed with a NAS 9060 computer. The atoms constituting the bleomycin–iron molecule were represented as 120 points; the carbon monoxide molecule was not incorporated in the calculations since the position of this ligand in the complex could not be established (vide infra). Also, the bithiazole–aminopropyl end of the molecule was not included in this representation since there was no evidence that it participated in iron binding (vide infra); on the contrary, all available evidence indicates that this part is attached as a flexible tail to the core of the molecule. Incorporated in the 120 points, however, were the hydrogen atoms attached to the carbon and nitrogen atoms. The structural information available for the iron–bleomycin complex was converted into distance constraints with defined upper and lower bounds. These constraints were derived as follows:

(a) All bond lengths and bond angles were allowed to vary over a range of 1% from their standard values.

(b) Torsion angles derived from the vicinal coupling constant analysis (vide infra) were fixed by constraining the 1,4 interpoint distances (within 1% range). This was done for the C_α–C_β part of the β-hydroxyhistidine fragment (H).

(c) Several parts of the bleomycin molecule have a rigid conformation. These are the aromatic pyrimidine and imidazole groups. Also the gulose and mannose sugars were considered rigid as for the bleomycin–zinc molecule.[17] These conformations were kept fixed by constraining all the interpoint distances concerned (within a 1% range). Thus, the sugar residues were only allowed to rotate around the glycosidic linkages, and in addition, the C_5–C_6 bonds were free to rotate.

(d) All amide bonds were considered to be planar/trans.

(e) The bleomycin molecule contains 19 asymmetric carbon atoms, but for each the configuration is known. The normal distance constraints obtained for those chiral centers do not discriminate between *R* and *S* configurations. Hence, a vector contribution to the error function was used such that optimization of this error function both ensured properly bounded distances and the correct chirality about each asymmetric carbon.[35] This vector contribution was also used to maintain the planarity of all sp^2 centers in the molecule.

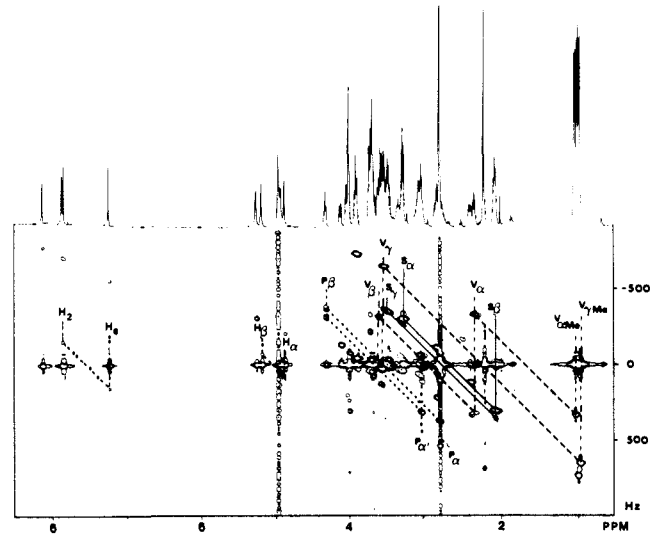

Figure 2. Contour plot of the 500-MHz SECSY spectrum of BLM–Fe–CO dissolved in D_2O recorded at 277 K during solvent irradiation. Connectivity pathways of threonine (T), β-hydroxyhistidine (H), bithiazole (B), and (γ-aminopropyl)dimethylsulfonium (S) are outlined. The subscripts, numbers and greek letters correspond with those in Figure 1.

(f) The iron binding sites were translated into distance constraints. They include the amine function of the β-aminoalanine fragment, the pyrimidine ring N_5 nitrogen, the β-hydroxyhistidinyl amide nitrogen, the imidazole ring N_1 nitrogen, and the carbamoyl nitrogen of the mannose sugar (Figure 1). The distances between the iron ion and these binding sites were set to 0.19–0.23 nm.

(g) The experimental data from the NOESY experiments (vide infra) were included in the distance constraints. The interpoint distance range between protons exhibiting NOE effects was uniformly set from 0.24 to 0.5 nm. In case NOE effects were observed with methyl protons, the interpoint distance range was set from 0.28 to 0.6 nm. This was necessary because the methyl groups were represented as point groups with a 0.1-nm radius.

(h) If nothing was known about the distance between two points, the lower bound was uniformly set to 0.24 nm and the upper bound to 2.5 nm. The latter value seemed reasonable for a molecule having the size of bleomycin.

Subsequently, all upper and lower bounds of the distance matrix thus derived were smoothed according to the triangular inequality. At this point, distances between all smoothed upper and lower bounds were selected and embedded in three-dimensional space. In this way a three-dimensional structure was generated. In general, such a structure will not satisfy the initial distance constraints, and final refinement has to be achieved in a minimalization routine. In this routine, a self-correcting conjugate gradient algorithm[36] is employed.

In every calculation 20 structures were generated. In order to reduce the calculation time, only 500 iterations were carried out in the final optimizing step of the distance geometry calculations.

Results and Discussion

^{1}H Assignments. The spin systems one expects to observe in a ^{1}H NMR spectrum for BLM dissolved in a D_2O solution are listed in Table I together with the fragments of the molecule and their abbreviations. Residues or groups of residues without (apparent) *J* couplings have not been incorporated in this list.

The ^{1}H NMR spectra of BLM–Fe–CO, recorded at 298 and 277 K, were studied, but in general, the discussion will be focused on the low-temperature spectrum because, below, the structure of the low-temperature complex will be determined. The strategy followed to perform the resonance assignments is completely analogous to the one we used in the interpretation of the ^{1}H NMR spectra of BLM[16] and BLM–Zn.[17] Therefore, only a brief discussion of the present assignments is given below.

The connectivity patterns that form the basis for the identification of the nonexchangeable protons are collected in the spin–echo correlated spectra presented in Figures 2–4. The cross

(31) Keeler, J.; Neuhaus, D. *J. Magn. Reson.* **1985**, *63*, 454.
(32) Muller, L. *J. Am. Chem. Soc.* **1979**, *101*, 4481.
(33) Bax, A.; Subramanian, S. *J. Magn. Reson.* **1986**, *67*, 565.
(34) Bax, A.; Summers, M. F. *J. Am. Chem. Soc.* **1986**, *108*, 2093.
(35) Crippen, G. M. *Distance Geometry and Conformational Calculations*; Bawden, D., Ed.; Research Studies Press: Chichester, England, 1981.
(36) Perry, A. *Int. J. Comp. Math.* **1978**, *B6*, 327.

Table I. Networks of Coupled Spins in Bleomycin A_2 in D_2O

abbr	fragment	spin system	
T	threonine	CH_3–CH–CH	A_3MX
P	pyrimidinylpropionamide	CH_2–CH	ABX
V	methylvalerate	CH_3–CH–CH–CH–CH_3	A_3MPTX_3
H	β-hydroxyhistidine	CH–CH	AX
A	β-aminoalanine	CH_2–CH	ABX
B	bithiazole	CH_2–CH_2	AA′XX′
S	(γ-aminopropyl)dimethylsulfonium	CH_2–CH_2–CH_2	AA′MM′XX′
G	α-L-gulose	CH–CH–CH–CH–CH–CH_2	
M	α-D-mannose	CH–CH–CH–CH–CH–CH_2	

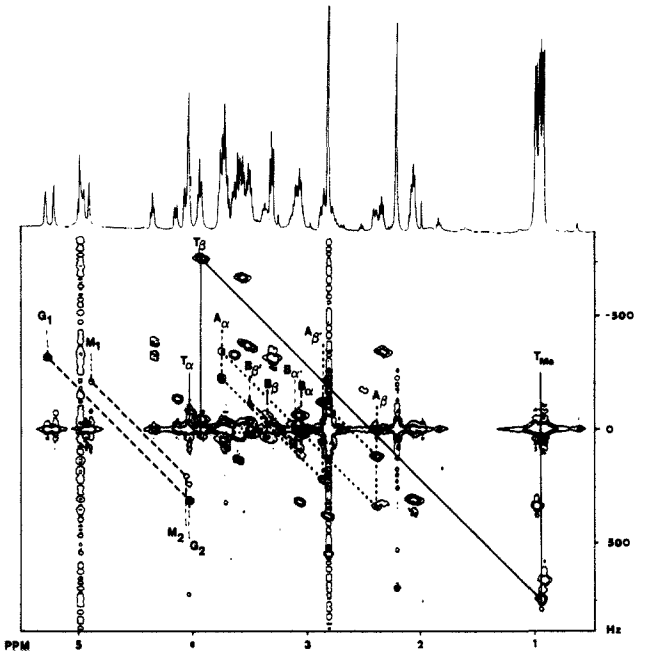

Figure 3. High-field region of the spectrum shown in Figure 2. The connectivity patterns of methylvalerate (V), β-aminoalanine (A), and pyrimidinylpropionamide (P) are indicated. Also shown are the H_1–H_2 correlations of the sugar fragments, α-L-gulose (G) and α-D-mannose (M).

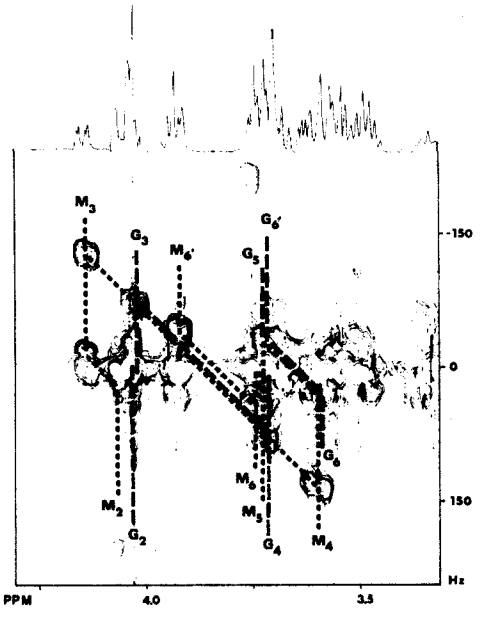

Figure 4. Connectivity "walks" of the mannose and gulose fragments (M, G) in the 500-MHz SECSY spectrum of BLM–Fe–CO in D_2O recorded at 277 K. The H_1–H_2 cross peaks are omitted in this figure (cf. Fig. 3).

peak patterns could be easily recognized on the basis of the knowledge already available from the ^1H spectra of BLM and BLM–Zn[16,17] except for those of the gulose and mannose moieties. The connectivity patterns of these two residues are drawn in Figure 4. Some of the resonances were readily assigned, namely, the mannose H_2, H_3, and H_4 as well as the gulose H_2 resonance, while others were more difficult to assign mainly because their positions are so close together. For instance the resonances G_4, G_5, and G_6, are nearly overlapping (cf. Figure 4). Nevertheless, assignments could be made by involving ^1H–^{13}C correlated spectroscopy (vide infra). We will return to this aspect in the following section.

Obviously, no cross peaks are observed for the resonances of the isolated spins of the bithiazole aromatic protons and the methyl groups of the pyrimidine ring and the dimethylsulfonium residue. The methyl groups are assigned on account of their intensity and position in the spectrum while both aromatic bithiazole protons can be assigned via the multiple-bond ^1H–^{13}C correlated spectrum, as will be discussed below.

The amide protons of the threonine, methylvalerate, bithiazole, and aminopropyldimethylsulfonium fragments can be identified with the aid of a double-quantum-filtered COSY spectrum recorded in H_2O (Figure 5). Cross peaks are observed between the amide proton resonances and the resonances of the nonexchangeable neighboring protons, which were identified in the procedure described above. Also, the position of the single secondary amine proton resonance (5.38 ppm) can be determined in this spectrum via cross peaks with the β-proton resonances of the pyrimidinylpropionamide and aminoalanine fragments. The primary amine functions of the aminoalanine and the pyrimidine fragment can only be assigned in a NOESY spectrum recorded in H_2O via cross peaks with the aminoalanine α-proton and the pyrimidinyl methyl resonances, respectively (cf. Figure 6). The resonances of the amine group of the β-aminoalanine are visible separately, while the amine group of the pyrimidinyl moiety shows only one resonance. As in the ^1H NMR spectrum of BLM–Zn,[17] the lowest field resonance (12.25 ppm; Figure 6) belongs to the imidazole NH function.

At this point we have not yet identified the resonances of the secondary amide protons of the aminoalanine, the pyrimidinylpropionamide, and the mannose moieties. Candidates for these protons are the six largest resonances between 5.5 and 9 ppm, which were not yet characterized. Their assignments were made in analogy with those in the BLM–Zn spectrum. Two sets of resonances can be distinguished on the basis of the connecting cross peaks and be assigned to the free amides of the aminoalanine and the pyrimidinylpropionamide residues. We could however not establish at this time which of the two cross peak patterns belongs to either the A or the P moiety (cf. Figure 6). The remaining two resonances (6.19 and 6.43 ppm) are assigned to the carbamoyl protons of the mannose residue. This assignment is somewhat ambiguous since in the 5.5–6.5 ppm region in the spectrum several broad resonances are observed. These could be due to hydroxyl protons whose exchange with water has been sufficiently slowed down in the complex (as a result of H bonds) to make them observable. The carbamoyl resonances are somewhat lesser broadened than in the BLM–Zn spectrum, but exchange with the solvent H_2O protons is still sufficiently rapid that in the 2D-NOE spectrum only the exchange cross peaks to the H_2O resonance and not the diagonal peaks are observed (Figure 6). Finally it is noted that the amide resonance of the hydroxyhistidinyl residue could not be traced in any of the spectra as for the BLM–Zn complex[17] but in contrast to the free BLM spectrum.[16]

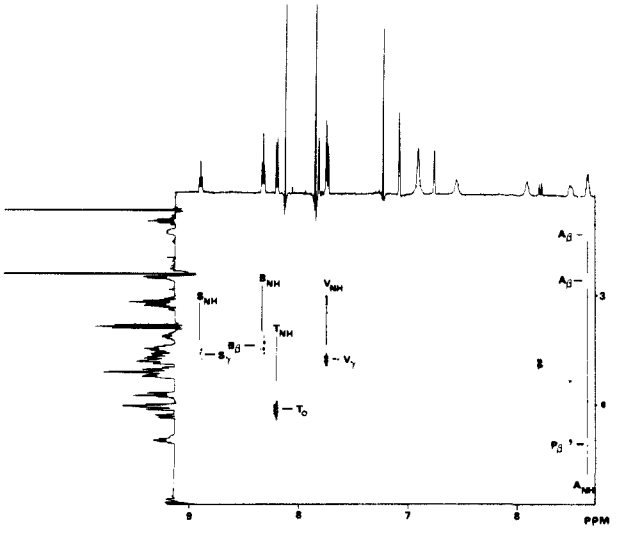

Figure 5. Part of the double-quantum-filtered COSY spectrum (ω_1 = 2.2–4.9 ppm. ω_2 = 5.3–9.2 ppm) recorded at 277 K for BLM–Fe–CO dissolved in H_2O. The solvent was irradiated moderately in order to reduce saturation of the exchangeable proton resonances in the spectrum. The cross peaks between the amide proton resonances and the resonances of the nonexchangeable neighbors are indicated. The meanings of the symbols are given in Table I and are the same as in Figures 2 and 3. Also, the cross peaks between the secondary amine resonance of the β-aminoalanine moiety (A_{NH}, 5.38 ppm) and the neighboring β resonances are indicated.

All ^1H assignments are summarized in Table II along with the BLM and BLM–Zn data.

^{13}C Assignments. The ^{13}C spectra were recorded at 298 K in D_2O. On inspection of the 1D ^{13}C spectrum of BLM–Fe–CO (Figures 7 and 8), one observes 53 separated resonances, while BLM–Fe–CO contains 56 carbon atoms. Since the methyl carbons of the dimethylsulfonium group are magnetically equivalent, one expects that three other carbon resonances overlap in the ^{13}C spectrum, which is indeed the case at 68.1 ppm. All carbon resonances can be assigned with the aid of ^1H-detected one-bond and multiple-bond ^1H–^{13}C correlated spectra (Figures 7–9). The one-bond correlated spectrum was recorded without carbon decoupling, which resulted in antiphase doublets (in the f_2 direction). The spectrum was recorded in this manner because we were also interested in the $^1J_{CH}$ couplings, which can be extracted from the antiphase doublets.

The assignments of all carbon resonances except for those arising from the quaternary carbons can be established in a rather straightforward manner (Figures 7 and 8) because every proton resonance in this spectrum is connected to the carbon resonance of the directly attached carbon atom via the doublet cross peaks. In the proton assignment section we showed that the assignment of the mannose H_2, H_3, and H_4 and the gulose H_2 protons was rather straightforward. Here, we can see that in the ^1H–^{13}C correlated spectrum in Figure 8, the positions of the sugar H_6 and $H_{6'}$ resonances (as well as the corresponding C_6 carbons) are readily derived via the characteristic cross peak patterns usually obtained for methylene fragments (one carbon resonance connected with two proton resonances). The assignment of these resonances to either the gulose or mannose sugar moiety follows from the characteristic J-coupling pattern of the mannose methylene fragment in the proton spectra, as in the case of the zinc complex. Now, only the mannose H_5 and the gulose H_3, H_4, and H_5 protons are not yet assigned. On account of the positions of the antiphase cross peaks in Figure 8, it is concluded that one sugar proton resonance has the same chemical shift position as both H_2 resonances. In combination with the connectivity patterns in a relayed coherence transfer (RCT) spectrum (not shown), this resonance is assigned to the gulose H_3 proton. Now, the position of the gulose H_4 proton follows directly from the SECSY spectrum shown in Figure 4. It is seen that this resonance has nearly the same chemical shift position as the mannose H_6 and the gulose $H_{6'}$

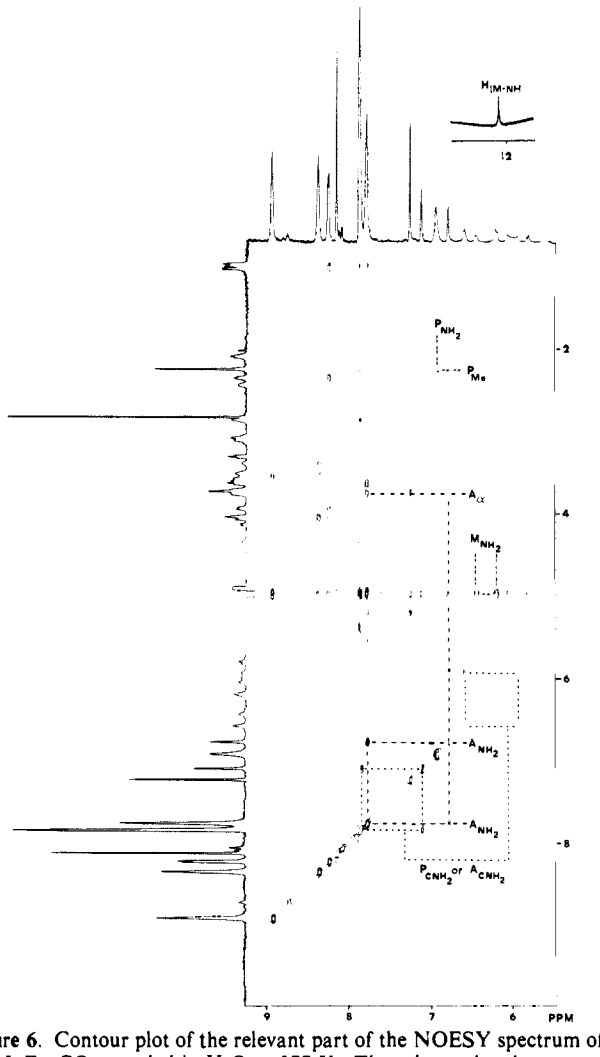

Figure 6. Contour plot of the relevant part of the NOESY spectrum of BLM–Fe–CO recorded in H_2O at 277 K. The solvent signal was suppressed with aid of a semiselective observation pulse (TSLONG) combined with a digital shift accumulation (DSA-4). As a result of the application of this method, saturation of the exchangeable proton resonances is avoided but resonances near the solvent signal are somewhat suppressed. The identification of several exchangeable protons is shown here. The free amide groups of the aminoalanine and propionamide residues are indicated by a subscript CNH_2 whereas the mannose carbamoyl group is denoted by NH_2.

resonances. Subsequently, the positions of both sugar H_5 protons can be established via the cross peaks in Figure 8 with the yet unassigned carbon resonances. Note that these proton resonances reside in the region of the proton spectrum where three sugar proton resonances were already assigned (M_4, M_6, $G_{6'}$). The assignments of carbon resonances M_4, M_5, and G_5 were established via a comparison with the ^{13}C spectra of free BLM and BLM–Zn.[18]

The multiple-bond ^1H–^{13}C correlated spectrum (Figure 9) shows more complicated cross peak patterns than the one-bond spectrum. Therefore, a detailed description of the quaternary carbon resonance assignments is presented. As an example, we shall first consider the quaternary carbons of the carbonyl groups of the primary and secondary amides and then those of the aromatic residues. All primary and secondary amide carbonyl carbon resonances display cross peaks with resonances of nonexchangeable neighboring protons. The secondary amide carbonyl carbon resonances of the pyrimidinylpropionamide and hydroxyhistidinyl fragments can be distinguished because the latter exhibits a very small cross peak (not shown) with the histidinyl β-proton resonance.

Subsequently, the aromatic carbon resonances of the pyrimidine, bithiazole, and imidazole fragments can be recognized via characteristic connectivity patterns with resonances of the protons

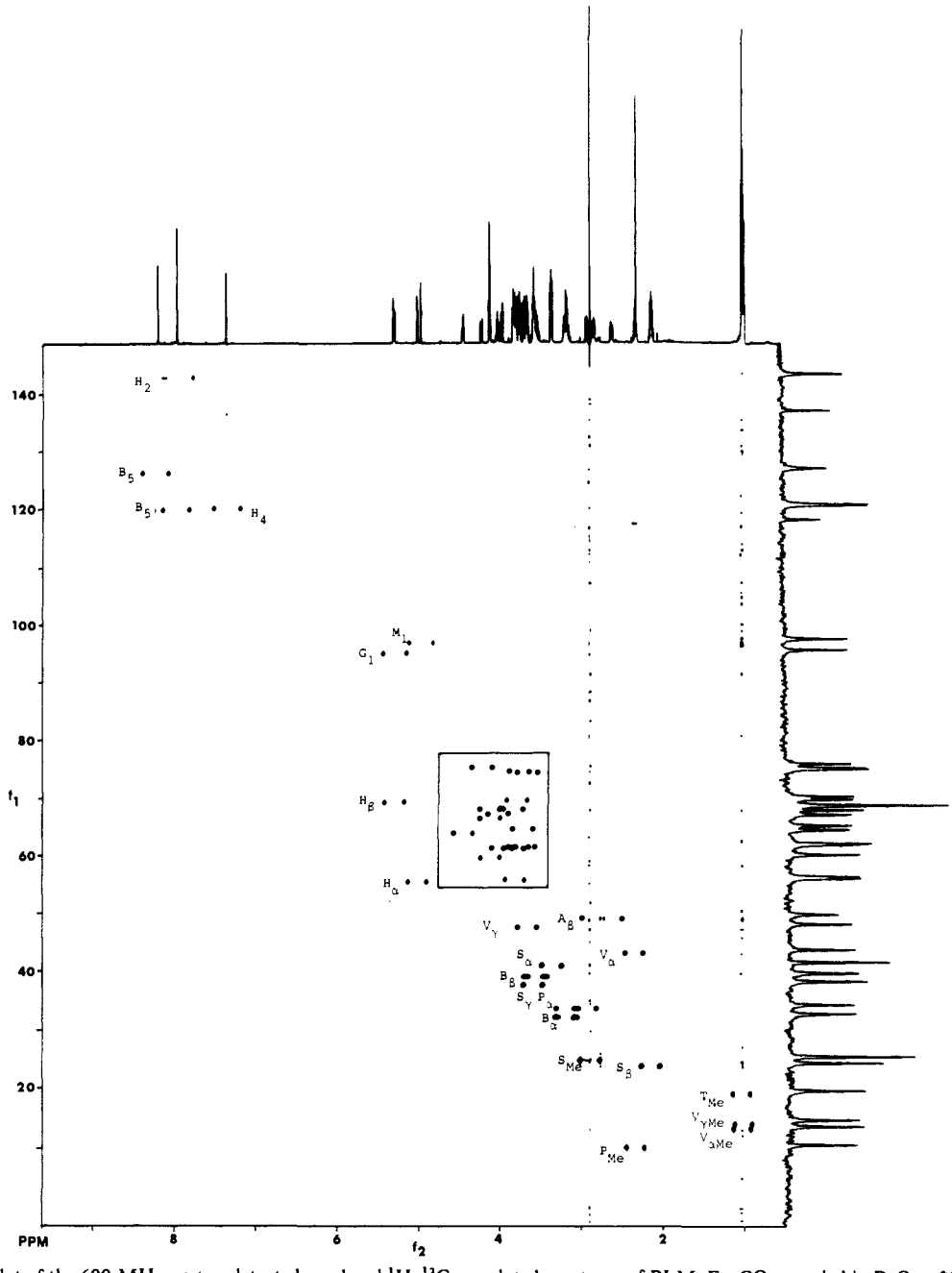

Figure 7. Contour plot of the 600-MHz proton-detected one-bond ^1H–^{13}C correlated spectrum of BLM–Fe–CO recorded in D_2O at 298 K. The spectrum was recorded without carbon decoupling. As a consequence, the ^1H–^{13}C correlations appear as doublets in which the components are separated by the $^1J_{CH}$ coupling. For reference purposes, a 200-MHz ^{13}C spectrum is presented along the ω_1 axis. The connectivities enclosed in the box are shown in more detail in Figure 8.

attached to these aromatic residues. Typically, the pyrimidine C_2, C_3, and C_4 resonances show cross peaks with the ^1H resonance of the methyl group of this residue (Figure 9). They can be distinguished on the basis of their chemical shift differences. Furthermore, the C_6 resonance of this residue can be assigned on account of cross peaks with the α- and β-protons of the propionamide fragment and a small cross peak with the pyrimidine methyl group protons (not shown). The imidazole C_5 resonance shows cross peaks with all proton resonances of the hydroxyhistidine fragment. Characteristically, the bithiazole $C_{2'}$ resonance can be recognized via cross peaks with the α- and β-proton resonances of this residue along with a connectivity to the aromatic $H_{5'}$ resonance. As a consequence, the aromatic protons (H_5 and $H_{5'}$) can now be distinguished in the proton spectrum. Having attained this information it is possible to assign the remaining quaternary bithiazole carbon resonances on the basis of cross peaks to the H_5 and $H_{5'}$ resonances.

Finally, by elimination, the yet unassigned low-field carbon resonance (218.9 ppm) must belong to the carbon monoxide. For this assignment, additional proof was obtained from a 1D ^{13}C spectrum of an enriched BLM–^{57}Fe–CO complex where a $^1J_{FeC}$ coupling (30 Hz) is observed between iron-57 and the carbon monoxide carbon atom (Figure 11). This establishes that this ligand is directly bound to the iron atom.

The ^{13}C assignments are summarized in Table III and compared to BLM and BLM–Zn data.

The Three-Dimensional Structure. With the elucidation of the ^1H and ^{13}C spectra of BLM–Fe–CO, the basis is provided for the three-dimensional structure determination of the complex. As is customary, this will be attempted by making use of available J coupling and NOE information. Thus, for D_2O and H_2O samples, NOESY spectra were recorded at 277 K with a mixing time of 400 ms (Figures 12 and 13). At this temperature positive cross peaks are observed, however with low intensity. This reflects the situation that, for the complex, $\omega\tau_c$ is close to unity (at 11.7 T). All nontrivial NOEs (i.e., excluding NOEs between geminal and vicinal protons) are numbered in Figures 12 and 13; they are listed in Table V.

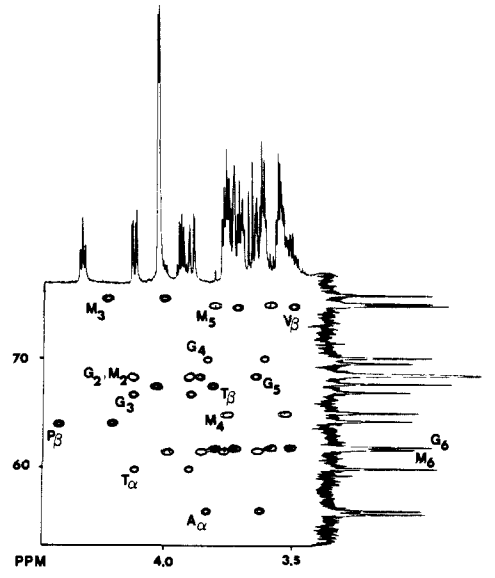

Figure 8. Part of the contour plot shown in Figure 7. The assignment of the cross peaks is indicated. For an explanation, see text. Around 61.5 ppm, double doublets are seen that are typical of the methylene groups of the mannose and gulose fragments (M_6 and G_6).

Inspection of Table V shows that most of the NOEs are identical with those observed for the BLM–Zn complex.[17] For instance, the NOEs observed for the sugar residues (NOEs 9–12 and 22 in Table V) were also recorded in the NOESY spectra of the BLM–Zn complex. It appears therefore that the conformation and orientation of the sugar moieties, with respect to each other and to the histidine residue, is the same in both complexes. This is true for other parts as well. For instance, the secondary amine group and the imidazole ring are directed toward each other, as is indicated by NOEs 23–26 (Table V). This is also the case in the BLM–Zn complex. Furthermore, no nontrivial NOEs are observed for the rest of the bithiazole fragment and the (aminopropyl)dimethylsulfonium part of the molecule, reflecting the larger flexibility of these moieties. Evidently, this part of the molecule is attached to the core as a flexible "tail", as in the BLM–Zn(II) complex. On the other hand, there are also some interesting differences. For the BLM–Fe–CO complex, no NOEs are observed between the aminoalanyl α-amine group and protons of other residues. Furthermore, the methylvalerate–threonine fragment generates some interesting interresidue NOEs (20 and 34 in Table V), which are absent in the NOESY spectra of the BLM–Zn complex.

Another important source of structural information is formed by the vicinal proton coupling constants. In our study of the BLM–Zn complex[17] we have shown that the torsional angles involving the C_α–C_β bond of the aminoalanine and hydroxyhistidine residues exist in a fixed conformation in the metal complex. When the vicinal coupling constants of this complex are compared with the corresponding coupling constants in the BLM–Fe–CO complex (Table IV, Figure 10), it is obvious that a major difference exists for the C_α–C_β conformation of the aminoalanine fragment. While in the hydroxyhistine residue in the BLM–Fe–CO complex the vicinal coupling constant is identical (3.2 ± 0.2 Hz) with that in the BLM–Zn complex, reflecting the same conformation, the vicinal coupling constants of the aminoalanine fragment increase significantly, as compared to those of the BLM–Zn complex, and approach those found in the metal-free BLM.[16] These results suggest that this part of the molecule has the conformational freedom of that in the metal-free BLM. Indeed, using a Karplus-like equation, which takes into account the electronegativity of the substituents at the C_α–C_β bond of the aminoalanine residue,[37] we could rule out the possibility that one

(37) Haasnoot, C. A. G.; De Leeuw, F. A. A. M.; Altona, C. *Tetrahedron* **1980**, *36*, 2783.

Table II. Resonance Positions of the Proton Signals of BLM-Fe–CO at pH 7, 277 K, and 298 K (Assignments Are Compared with BLM and BLM–Zn Data)

		chemical shifts, ppm					chemical shifts, ppm					chemical shifts, ppm		
		metal-free	zinc-bound	iron-bound			metal-free	zinc-bound	iron-bound			metal-free	zinc-bound	iron-bound
frgmt	group	297 K	277K	298 K	frgmt	group	297 K	277K	298 K	frgmt	group	297 K	277K	298 K
T	CH_3	1.085	1.021	1.04	A	$C_\alpha H$	3.84	3.724	3.80	G	C_1H	5.251	5.305	5.28
	$C_\alpha H$	4.207	4.099	4.11		$C_\beta H$	2.83	2.458	2.60		C_2H	4.013	4.063	4.08
	$C_\beta H$	4.075	3.999	4.00		$C_\beta H'$	2.88	3.356	2.85		C_3H	4.09	4.03	4.08
	NH		7.96			sec NH		4.32			C_4H	3.84	3.71	3.78
P	$C_\alpha H$	2.62	2.871	2.93		prim NH_2		6.94			C_5H	3.99	3.849	3.82
	$C_\alpha H'$	2.69	3.244	3.18		prim NH_2		7.36			C_6H	3.40	3.606	3.66
	$C_\beta H$	3.958	4.498	4.43		amide NH_2		7.12/5.92	7.08/5.93		C_6H'	3.53	3.69	3.76
	ring CH_3	2.009	2.376	2.33		amide NH_2		7.89/6.56	7.83/6.57	M	C_1H	4.994	4.885	4.95
	ring NH_2		7.02		B	$C_\alpha H$	3.24	3.16–3.18	3.08		C_2H	4.04	4.079	4.11
	amide NH_2		5.92/7.12	5.93/7.08		$C_\alpha H'$			3.12		C_3H	4.675	4.03	4.21
	amide NH_2		6.56/7.89	6.57/7.83		$C_\beta H$	3.60	3.51–3.55	3.35		C_4H	3.78	3.67	3.70
V	α-CH_3	1.100	0.982	1.03		$C_\beta H'$			3.51		C_5H	3.78	3.70	3.74
	γ-CH_3	1.116	0.934	0.96		ring C_5H	8.199	8.207	8.11		C_6H	3.78	3.787	3.81
	$C_\alpha H$	2.452	1.946	2.36		ring C_5H	8.004	8.037	7.85		C_6H'	3.918	3.965	3.97
	$C_\beta H$	3.703	3.415	3.64		NH		8.36	8.33		NH_2		6.00	6.19
	$C_\gamma H$	3.863	3.615	3.58	S	$C_\alpha H_2$	3.377	3.357	3.31		NH_2		6.38	6.43
	NH		7.55	7.75		$C_\beta H_2$	2.163	2.134	2.09					
H	$C_\alpha H$	5.052	4.851	4.93	4.99	$C_\gamma H_2$	3.60	3.572	3.53	3.58				
	$C_\beta H$	5.257	5.196	5.19	5.28	sulf $(CH_3)_2$	2.909	2.878	2.83	2.89				
	ring C_2H	7.786	8.037	7.86	7.92	NH		8.94	8.90					
	ring C_4H	7.261	7.305	7.23	7.32									
	ring NH		12.45	12.25										

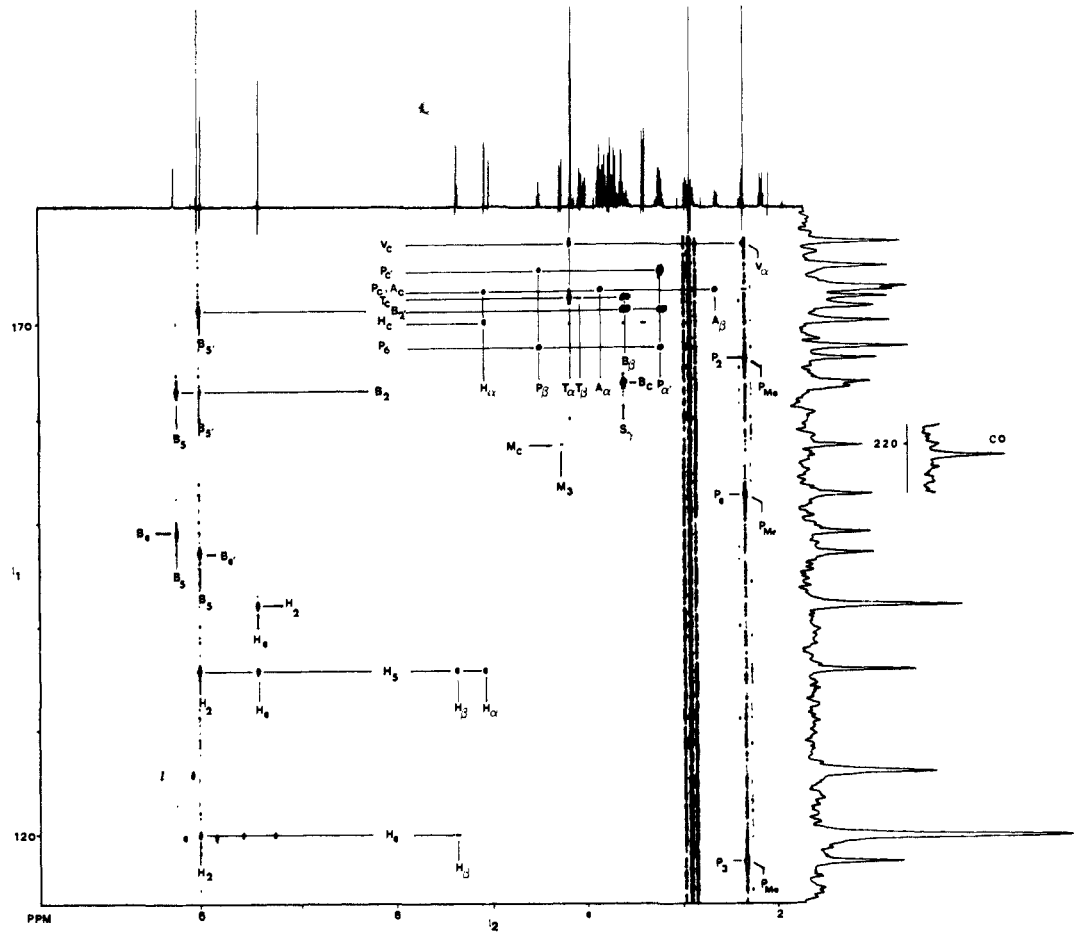

Figure 9. Relevant part of the 600-MHz proton-detected multiple-bond ^1H–^{13}C correlated spectrum of BLM–Fe–CO in D_2O recorded at 298 K. For reference purposes, a 200-MHz ^{13}C spectrum is shown along the ω_1 axis. All quaternary carbon resonance assignments are outlined in this figure. The abbreviations along the horizontal and vertical lines correspond to carbon and proton resonances, respectively.

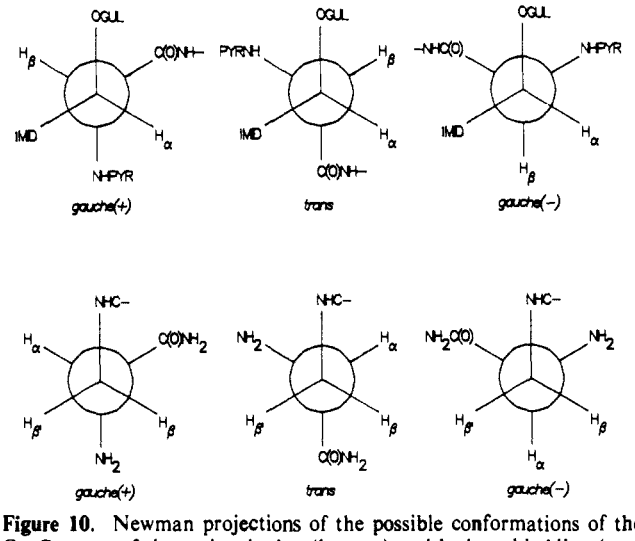

Figure 10. Newman projections of the possible conformations of the C_α–C_β parts of the aminoalanine (bottom) and hydroxyhistidine (top) residues. The following abbreviations are used: Pyr, pyrimidinyl; Imid, imidazole; Gul, gulose.

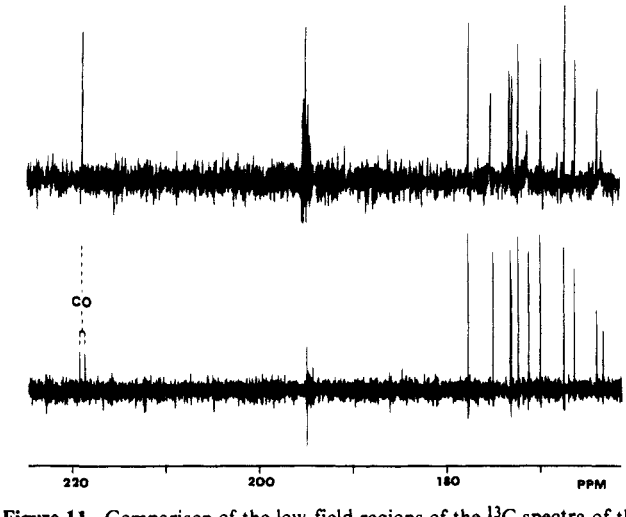

Figure 11. Comparison of the low-field regions of the ^{13}C spectra of the BLM–Fe–CO complex (top) and the enriched BLM–^{57}Fe–CO complex (bottom). A 30-Hz $^1J_{FeC}$ coupling is observed between iron-57 and carbon monoxide (218.9 ppm), indicating the existence of a σ bond between the metal ion and the carbon monoxide carbon.

single conformation (even if nonstaggered) is able to account for the observed coupling constants. Yet the existence of an almost 1:1 mixture of slightly nonstaggered well-defined gauche (–) and trans conformers requires consideration, and we will elaborate upon this shortly.

The NOEs and the fixed torsional angle of the hydroxyhistidinyl C_α–C_β part of the complex were translated into a three-dimensional structure via distance geometry calculations.[35] In the calculations, the atoms constituting the BLM molecule were represented as 119 points. In this representation, the bithiazole–(aminopropyl)dimethylsulfonium end of the molecule was disregarded since it is largely flexible (vide supra). At this point, the metal ion and the carbon monoxide molecule were excluded from the calculations as well. In every calculation 20 structures were generated of which about 10 converged into so-called low-error structures, which were regarded as such when having a root mean square deviation from the initial distance constraints of less than 0.003 nm. In Figure 14, four of such low-error structures are shown. The structure of the histidine–gulose–mannose fragment is well described by the NOEs and the torsional angle, as is

Table III. Resonance Positions of the ^{13}C Signals of BLM–Fe–CO. The Assignments Are Compared to BLM and BLM–Zn Data

		chemical shifts, ppm					chemical shifts, ppm					chemical shifts, ppm		
frgmt	group	metal-free	zinc-bound	iron-bound	frgmt	group	metal-free	zinc-bound	iron-bound	frgmt	group	metal-free	zinc-bound	iron-bound
T	CH_3	19.3	19.3	19.3	H	C_α	57.3	61.1	55.6	S	C_α	41.3	41.3	41.3
	C_α	59.5	59.5	59.7		C_β	73.4	70.6	69.2		C_β	24.0	24.0	24.1
	C_β	67.4	67.4	67.3		ring C_4	118.0	118.2	119.8		C_γ	38.0	38.0	38.1
	C=O	172.4[a]	172.2[a]	172.4		ring C_5	135.2	135.5	135.9		sulf $(CH_3)_2$	25.0	25.1	25.1
P	C_α	40.6	33.9	34.1		ring C_2	137.3	137.8	142.2	G	C_1	97.8	95.6	94.9
	C_β	60.1	56.1	64.0		C=O	169.4	172.0	170.0		C_2	70.6	68.3/68.4	68.1
	ring CH_3	11.2	11.1	10.0	A	C_α	53.0	52.5	55.9		C_3	68.2	66.6	66.6
	ring C_3	112.6	114.2	117.2		C_β	47.8	45.0	49.4		C_4	69.5	70.1	69.7
	ring C_4	152.5	148.4	153.1		C=O	172.3	173.8	173.4		C_5	67.4	67.7	68.1
	ring C_2	165.0	168.0	166.4	B	C_α	32.4	32.4	32.5		C_6	60.6	61.6	61.6
	ring C_6	165.7	161.6	167.5		C_β	39.4	39.6	39.5	M	C_1	98.5	97.2	96.7
	HNC=O	168.0	169.3	173.1		ring $C_{5'}$	119.4	119.5	119.6		C_2	68.7	68.3/68.4	68.1
	H_2NC=O	176.5	176.6	175.4		ring C_5	125.5	125.5	126.0		C_3	74.7	75.5	75.3
V	α-CH_3	12.3	12.1	13.2		ring $C_{4'}$	147.3	147.3	147.3		C_4	65.1	64.5	64.7
	γ-CH_3	15.1	15.0	14.3		ring C_4	149.1	149.1	149.4		C_5	73.9	74.7	74.6
	C_α	43.0	43.0	43.4		ring C_2	163.0	163.1	163.6		C_6	61.3	61.3	61.4
	C_γ	47.9	47.3	47.8		ring $C_{2'}$	170.9[a]	171.0[a]	171.5		C=O	158.3	157.7	157.8
	C_β	74.7	74.7	74.4		C=O	163.7	163.7	164.0	CO				218.9
	C=O	177.8	177.6	177.8										

[a] The ^{13}C resonance positions of $T_{C=O}$ and $B_{C2'}$ were wrongly assigned in our study on BLM and BLM–Zn[18].

Table IV. Rotamer Populations of the C_α–C_β Parts of the Fragments H and A of BLM, BLM–Zn and BLM–Fe–CO[a]

		rotamer popultn, %		
fragm	^3J, Hz	g^+	t	g^-
	Bleomycin			
H	5.8 ± 0.2			
A	7.2 ± 0.2	50	23	27
	5.2 ± 0.2	31	60	9
	Bleomycin–Zinc			
H	3.1 ± 0.2		>90	
A	3.8 ± 0.2			100
	2.0 ± 0.2			100
	Bleomycin–Iron			
H	3.1 ± 0.2		>90	
A	7.2 ± 0.2	13	52	35
	4.2 ± 0.2	50	12	38

[a] The nomenclature g^-, g^+ or t refers to the backbone of the molecule. The possible conformations are shown in Figure 10.

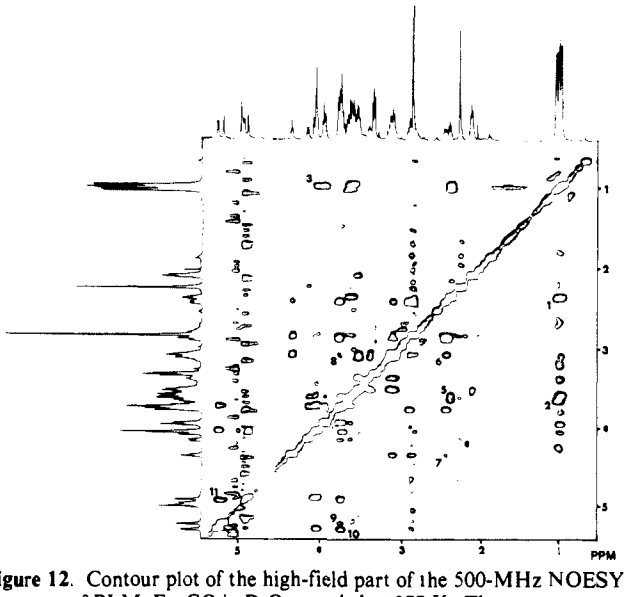

Figure 12. Contour plot of the high-field part of the 500-MHz NOESY spectrum of BLM–Fe–CO in D_2O recorded at 277 K. The spectrum was recorded with selective irradiation of the HDO resonance. Nontrivial NOEs are indicated according to the numbering in Table V.

indicated by the small conformational space to which these groups are constrained by the calculations. Furthermore, this conformation is virtually identical with the structure of this fragment in the BLM–Zn complex.[17] The conformation of the other parts of the BLM molecule are less well defined, and their mutual orientation as well as their orientation with respect to the histidine–sugar region cannot be established with sufficient accuracy. Obviously, this is due to a lack of interresidue NOEs toward the rest of the molecule. It is noted that in this respect the pyrimidine ring acts as a "NOE barrier" because the only protons attached to this group are the methyl protons.

A further definition of the molecular conformation can be obtained if the BLM ligation sites of the Fe(II) ion are known.

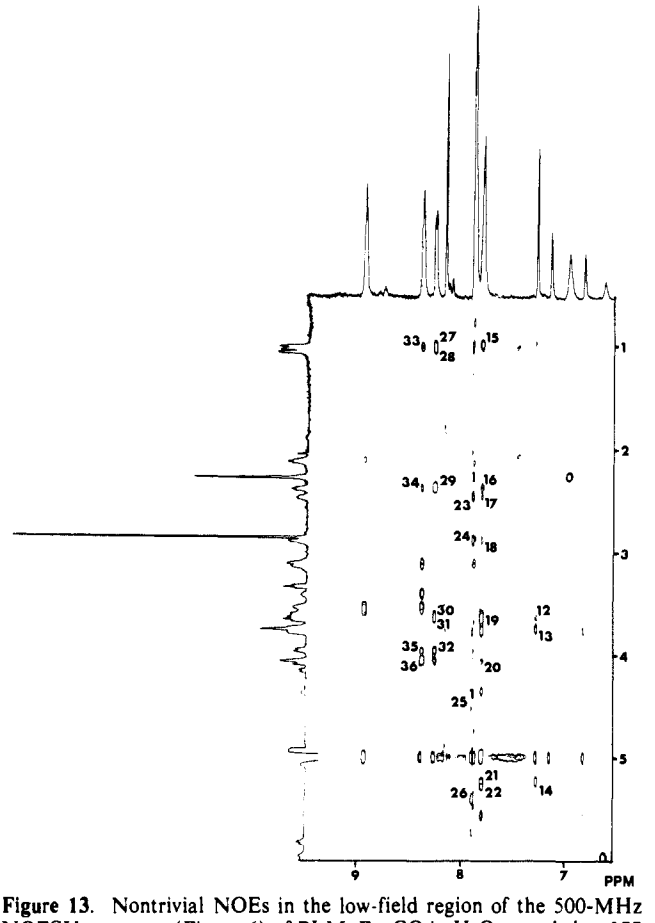

Figure 13. Nontrivial NOEs in the low-field region of the 500-MHz NOESY spectrum (Figure 6) of BLM–Fe–CO in H_2O recorded at 277 K. The NOEs are listed in Table V.

Table V. Nuclear Overhauser Enhancements Observed in the NOESY Spectra in Figures 12 and 13[a]

no.	NOE	no.	NOE	no.	NOE	no.	NOE
1	$V_{\gamma Me}$–V_α	10	G_1–M_5	19	V_{NH}–V_β	28	T_{NH}–$V_{\alpha Me}$
2	$V_{\alpha Me}$–V_β	11	G_1–H_α	20	V_{NH}–T_α	29	T_{NH}–V_α
3	T_{Me}–T_α	12	H_{H4}–G_6	21	V_{NH}–H_β	30	T_{NH}–V_γ
4	P_{Me}–M_3	13	H_{H4}–G_5	22	V_{NH}–G_1	31	T_{NH}–V_β
5	V_α–V_γ	14	H_{H4}–H_β	23	H_{H2}–A_β	32	T_{NH}–T_β
6	A_β–$P_{\alpha'}$	15	V_{NH}–$V_{\gamma Me}$	24	H_{H2}–$A_{\beta'}$	33	B_{NH}–T_{Me}
7	A_β–P_β	16	V_{NH}–V_α	25	H_{H2}–P_β	34	B_{NH}–V_α
8	$P_{\alpha'}$–A_α	17	$A_{NH2'}$–A_β	26	H_{H2}–A_{NH}	35	B_{NH}–T_β
9	G_5–H_β	18	$A_{NH2'}$–$A_{\beta'}$	27	T_{NH}–T_{Me}	36	B_{NH}–T_α

[a] Numbers correspond to those in Figures 12 and 13. Only nontrivial NOEs are listed.

In a first approximation we tried to establish these through the detection of J couplings, which could possibly be generated by the ^{57}Fe spin (^{57}Fe has a spin of $^1/_2$) in ^{15}N, ^{13}C, and ^{1}H spectra of a BLM–^{57}Fe–CO complex. However, except for the CO molecule (Figure 11), we failed to detect any, probably because the coupling constants are too small (for instance, in general, ^{57}Fe–^{15}N ^1J couplings are of the order of 6–8 Hz[38]). In a different approach one can try to make use of the chemical shifts induced by the presence of the metal ion. In the ^{1}H spectra, the most important changes in resonance positions [proceeding from the metal-free BLM to the BLM–Fe(II)–CO complex] occur for the same protons as in the BLM–Zn(II) complex, except for the Val C_αH and one of the Ala C_βH resonances, which exhibit shifts that are considerably smaller in the Fe(II)–CO complex (cf. Table II).

As we and others had observed already for the BLM–Zn(II) complex, the complexation shifts of the ^{13}C resonances may be considerably larger.[17] This is also observed for the Fe(II)–CO complex. However, upon inspection of the ^{13}C chemical shifts (Table III) of the BLM–Fe–CO complex and those of the metal-free BLM and the BLM–Zn molecule,[18] it is evident that it is not always straightforward to derive metal coordination sites from these chemical shift differences, e.g., some shifts that were negative upon complex formation with Zn(II) are positive in the Fe(II)–CO complex and vice versa. Yet, on the basis of the large chemical shift changes induced upon complexation with the metal ion, the pyrimidine and imidazole groups can be assessed as chelators of the iron ion. Unfortunately, the other chemical shift changes cannot simply be translated into iron ligating sites. However, it seems safe to conclude that the fragments methylvalerate, threonine, bithiazole, and (aminopropyl)dimethylsulfonium are not actively participating in metal binding since the ^{13}C chemical shift differences as compared to the metal-free BLM are small. The same conclusions follow from the ^{1}H shifts, and they match those obtained earlier.[17]

As discussed already (vide supra), the conformation of the sugar moieties and the histidine group is well defined by the experimentally available torsion angle and NOEs. In this structure, the nitrogen atom of the histidine amide is directed toward the imidazole N_1 atom, which is a metal binding site (vide supra). Juxtaposition of these two atoms can only be maintained if the histidine amide nitrogen is anchored to the metal ion. Therefore, as in our study of the BLM–Zn complex, we consider the amide of this fragment to be bound to the Fe(II) ion. This conclusion is supported by the absence of the amide proton resonance in the H_2O spectra, indicating that upon metal binding the amide is deprotonated and therefore a convenient chelator of the Fe(II) ion. We recall that this resonance is observed in the spectra of the metal-free BLM at the same solution conditions,[16] while it is also absent in the spectra of BLM–Zn.[17] A similar reasoning is applicable to the sugar moieties. The mannose group adopts a specific orientation with respect to the imidazole group. Again, this orientation can only be maintained if the mannose group is anchored to the metal ion. Combining this result with the shift of the mannose H_3 proton upon complexation, we conclude that

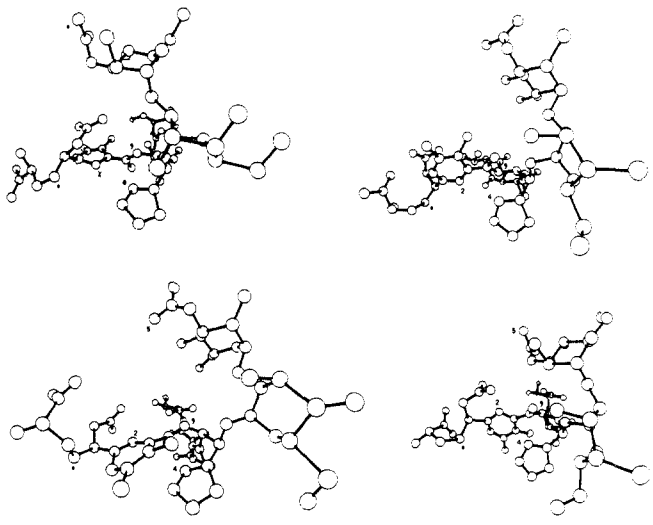

Figure 14. Four conformers of BLM satisfying the NOE and torsion angle distance constraints found in the spectra of the BLM–Fe–CO complex. The metal ion (and its constraints) were not included in the calculations. The numbered atoms correspond with those in Figure 1 that are marked with italic numbers.

it is the mannose carbamoyl group that is coordinated to the iron(II) ion. We cannot, however, differentiate between the ligation of the carbamoyl nitrogen or oxygen atom. It is noteworthy that it is unlikely that the gulose and mannose groups adopt the specific conformation when not actively involved in metal coordination, since in the spectra of the metal-free BLM there are no indications for interactions between the gulose and mannose and other groups in the molecule.

We have mentioned already that in the NOESY spectra recorded for a H_2O solution, NOE cross peaks connect the aminoalanyl secondary amine proton (and its neighbors) to the imidazole C_2H. This observation can only be explained if the secondary amine nitrogen is also participating in metal ion binding. It is noted in passing that these NOEs alone do not suffice to determine the orientation of the β-aminoalanine fragment with respect to the well-defined structure of the sugar–imidazole part of the molecule as followed from the distance geometry calculations discussed above (cf. Figure 14). We already mentioned that the pyrimidine ring is also involved in the interaction with the metal ion. Given the coordination to the metal ion of the histidine amide nitrogen and the secondary aminoalanine nitrogen, this can only take place through the binding of the N_5 ring atom. This could be confirmed by means of ^{15}N NMR spectroscopy (not shown).

At this point we have obtained five coordination sites for the metal ion. The sixth site is formed by the CO molecule, as is demonstrated by the observation of the coupling constant J_{FeC} (30 Hz) between iron-57 and the carbon monoxide carbon atom in the BLM–^{57}Fe–CO complex (vide supra, Figure 11). The value of 30 Hz indicates the existence of a σ bond between iron and the CO molecule.[39] With this additional information the distance geometry calculations were repeated. In this case, the BLM complex was represented by 120 points, i.e., compared to the calculations discussed above the metal ion was included as the 120th point. The five BLM sites that bind to the iron ion, i.e., the secondary amine, the pyrimidine N_5, the histidinyl amide nitrogen, the imidazole N_1, and the carbamoyl nitrogen, were constrained between 0.19 and 0.23 nm from the metal ion (cf. Materials and Methods). These constraints were introduced after inspection of known iron–nitrogen distances in crystal structures of several iron complexes. The NOE and the torsional angle constraints were used as in the aforementioned calculations (vide supra). Furthermore, the metal ion was constrained in the planes of the pyrimidine and imidazole ring systems. We note explicitly that the methylvalerate and threonine groups were incorporated

(38) Morishima, I.; Inubushi, T.; Sato, M. *J. Chem. Soc., Chem. Commun.* **1978**, 106.

(39) Jenny, T.; von Philipsborn, W. *J. Organomet. Chem.* **1981**, *205*, 211.

in the calculations. This was not the case with the bithiazole and (aminopropyl)dimethylsulfonium moieties, which were excluded from the calculations since, as mentioned already, the structure of these parts is not well-defined because of their flexibility. Also, the carbon monoxide was omitted since no information could be obtained as to the position of this molecule with respect to the other residues in the complex. Finally, we mention that the primary amine of the aminoalanine residue was not incorporated as a metal ion binding site; we will elaborate upon this presently. As in the calculations carried out without the metal ion, for every calculation 20 structures were generated of which about 10 converged to low-error structures that had a root mean square deviation of less than 0.003 nm from the initial distance constraints. In Figure 15, four of the low-error conformers resulting from these calculations are presented; they compose a family of conformations representing the solution structure of the BLM–Fe–CO complex in an aqueous environment. The figure has been drawn in such a way that the orientation of the methylvalerate–threonine fragment stands out with respect to the part of the BLM molecule ligated to the metal ion. Inspection of Figure 15 shows that for the different structures the orientation of the methylvalerate and threonine moieties may change significantly with respect to the core of the molecule, while the conformation of this dipeptide is constrained to a smaller space. In Figure 16, the four structures have been drawn in a different orientation while the methylvalerate and the threonine fragments have not been incorporated, so as to provide a clearer picture of the metal coordination. For the sake of clarity the protons have been omitted in the figures and the radius of the iron ion was slightly exaggerated. All calculated low-error conformers have root mean square distance deviations with respect to each other of less than 0.11 nm (this includes the methylvalerate and threonine groups). It is evident from Figure 16 that introduction of the constraints that keep the chelation sites attached to the metal ion causes the aminoalanyl–pyrimidine part of the complex to be confined to a smaller conformational space than that shown in Figure 14. The conformation of the hydroxyhistidine–sugar part of the complex, including three proposed metal binding sites (imidazole, histidine amide, and carbamoyl), is virtually the same as that in Figure 14. This means that the distance constraints introduced for the metal–nitrogen bonds of the histidine and mannose moieties correspond well with those introduced on the basis of the observed NOEs and J coupling for this part of the molecule. In other words, the proposed metal binding sites are in fact already defined by the NOEs and the fixed torsional angle, as we suggested above for the histidine amide and the carbamoyl group (vide supra).

It can be gleaned from Figure 16 that a possible coordination site for the carbon monoxide molecule is formed in a position apical to the mannose carbamoyl function resulting in a distorted octahedral coordination geometry around the iron ion.

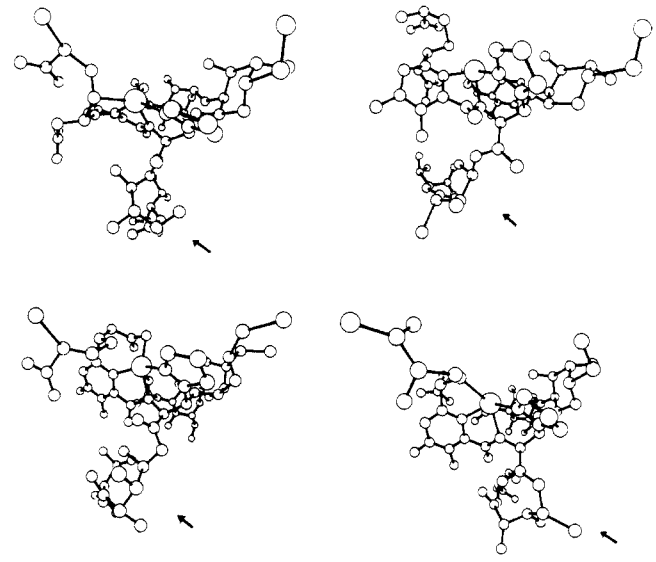

Figure 15. Four conformers of BLM–Fe–CO satisfying all available distance constraints (including the metal ion–nitrogen constraints). The hydrogen atoms are excluded for clarity. For the same reason the radius of the iron ion is exaggerated. The arrows indicate the position of the methylvalerate and threonine residues.

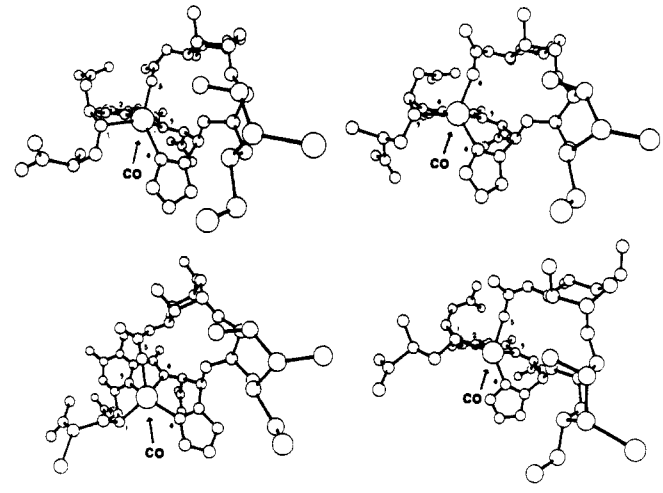

Figure 16. The conformers of BLM–Fe–CO in Figure 15 viewed from a different angle in order to get a clearer picture of the metal ion coordination. The hydrogen atoms are excluded for clarity as well as the fragments V, T, B, and S. For the same reason the radius of the iron ion is exaggerated. A possible position of the CO molecule is indicated with an arrow. The numbered atoms correspond with those in Figure 1 that are marked with italic numbers.

Discussion

A major part of the structure, derived in this paper for the BLM–Fe(II)–CO complex, has the same conformation as that obtained earlier for the BLM–Zn(II) complex.[17] The main difference between the complexes is the replacement of the primary amine function of the β-aminoalanine group, which binds to the metal ion in BLM–Zn(II), by the carbon monoxide in the Fe(II)–CO complex. As a result, a more symmetric structure with an octahedral-type conformation can be formed. In the BLM–Fe(II)–CO complex the nitrogen atoms of the secondary amine function, the pyrimidine and imidazole groups, and the histidine amide are, roughly speaking, located in a square with the metal ion in the center of the plane, whereas in the zinc adduct this situation cannot be obtained because the primary amine group is coordinated to the metal ion and thereby distorts the square-plane metal surroundings.

In this respect we note also that distance geometry calculations were performed in which the metal ion was not constrained in the planes of the pyrimidine and imidazole groups. This enlarged the conformational space of the pyrimidine moiety in the sense that the metal ion does not always remain in the plane of this group. Obviously, this is due to the lack of NOE constraints of this group toward the rest of the molecule, as already mentioned. These results, however, do not affect the aforementioned symmetry considerations.

Another difference between the BLM–Fe(II)–CO complex and the BLM–Zn(II) structure should be mentioned. In the former compound the methylvalerate–threonine part of the BLM seems more structured than in the zinc adduct. Moreover, it is not as close to the imidazole group as in the Zn(II) complex. At this moment, we have no explanation for these observations.

Comparison with Structure Proposals from Other Groups. We have now come to a point where it is necessary to compare the structure derived in this paper with proposals made earlier for the BLM–Fe(II)–X complex (where X = CO, NO, etc.). This is important because in most if not all of these proposals the primary amine function of the β-aminoalanine group is binding to the metal ion, while we did not (or to a limited extent) involve this function in metal coordination (vide infra). There is consensus about the coordination of three sites, namely, the secondary amine of the β-aminoalanine group, the N_5 atom of the pyrimidine ring,

and the imidazole N_1 function. The coordination of these sites follows from the present experiments as well. The other two BLM coordination sites for the Fe(II) ion that we derived from our results, namely, the mannose carbamoyl group and the histidine amide nitrogen, have also been indicated by other investigators. There are, however, two schools of thought, one of which has the carbamoyl group attached to the Fe(II) ion and not the histidine amide function but instead the primary amine group of the β aminoalanine fragment,[15] while the other group of investigators include the histidine amide group in the interaction with the metal ion instead of the carbamoyl moiety but also involve the primary amine function in metal chelation.[13,40-43] The latter conclusions were based on ESR experiments on BLM and analogues, including the deglycosylated deglyco-BLM, dep-BLM (lacking the alanine portion), and deamido-BLM, (having the alanine amide hydrolyzed). The ESR parameters of the nitrosyl adducts of Fe(II)-BLM and deglyco-BLM-Fe(II) are almost identical.[42] This has been interpreted to indicate that the carbamoyl group plays no role in coordination, in contrast to our results and those of the abovementioned other group of investigators: NMR studies by Oppenheimer et al. clearly demonstrated that the geometry in the deglyco-BLM-Fe(II)-CO complex differs substantially from that of the native BLM-Fe(II)-CO complex.[15,44] If these Fe(II)-CO complexes are directly comparable to the corresponding Fe(II)-NO complexes, as has been assumed, the conclusions derived from the ESR data do not necessarily hold. The conclusion of Oppenheimer et al. that the carbamoyl group binds to the metal ion was based on the large shift observed for the mannose H_3 resonance occurring upon complexation of BLM with the metal ion. This shift was also observed by us and used in support of the binding of the carbamoyl group (which is attached at the 3′ position of the mannose sugar) to the metal ion. Our main reason for deciding on this binding was, however, based on the finding that the sugar-histidine part of the molecule is well structured as soon as the Fe(II) ion is bound to the molecule. As pointed out above, this can only be rationalized if the carbamoyl group forms a chelation site.

However, in contrast to Oppenheimer et al., we have the histidine amide attached to the Fe(II) ion and not the primary amine function of the β-aminoalanine group. The Oppenheimer group did not give explicit reasons for not involving the histidine amide function other than that of elimination because there were already six chelating groups binding to the metal ion. We have very good reasons to involve this group in metal binding. Only in this way can its orientation be maintained with respect to the imidazole-sugar part of the molecule as it also was in the BLM-Zn(II) complex[17] (vide supra).

At this point we might, by elimination, exclude the primary amine function of the β-aminoalanine residue from metal coordination. This is indeed indicated by the coupling constants measured for the $CH-CH_2$ moiety of this residue. They increased from 3.8 and 2.0 Hz in the BLM-Zn(II) complex, where they characterize a well-defined structure, to 7.2 and 4.2 Hz in the BLM-Fe(II)-CO complex (cf. Table IV). This suggests a flexibility of the β-aminoalanine tail equivalent to that found in the metal-free BLM. We disagree with Oppenheimer et al. that the latter set of coupling constants may characterize a well-defined nonstaggered conformation.[15] Modern J coupling analysis with well-tested Karplus equations, which include electronegativity effects of substituents,[37] shows that this is not possible. We cannot dismiss, however, the possibility that the primary amine binds transiently to the metal ion, as a result of which two different geometries of the complex are temporarily formed. The necessary concomitant rearrangement of the other ligating groups is, however, not manifest in the spectra so that we consider this possibility somewhat unlikely.

It has been suggested in the literature[45,46] that the methylvalerate moiety, in particular the hydroxyl or carbonyl group, could also be involved in metal coordination. Such conclusions were based on the sensitivity of the α-CH resonance position of the methylvalerate residue in the NMR spectrum of the BLM-Zn(II) complex[47] and on more spectacular shifts observed in the NMR spectrum of the paramagnetic BLM-Fe(II) complex,[45] where the methylvalerate α-CH resonance position changes by about 40 ppm, as does the imidazole H_4 resonance. This behavior does not necessarily mean, however, that the valerate fragment is coordinated to the metal ion. Analysis of our BLM-Zn(II) structure[17] shows that in a number of our low-error structures the distance of the valerate α-CH proton to the zinc ion is about the same as that of the histidine H_4 proton of the metal ion bound histidine (~0.55 nm). Thus, while the valerate group is not coordinated to the metal ion, large shifts may still be observed in the NMR spectrum of the BLM-Fe(II) complex because of the apparent proximity of this proton to the metal ion.

It is interesting to add that the shift observed for the mannose M3H resonance of the paramagnetic BLM-Fe(II) complex is −14.8 ppm.[45] In the BLM-Zn(II) complex this proton is about 0.43 nm removed from the metal ion. Since the largest positive paramagnetic shifts are observed for the P CH_2, His H_4, and Val α-CH resonances, the main principal axis of the paramagnetic susceptibility tensor is roughly in the direction of the line that can be drawn through the Zn(II) ion and these protons. This axis and the line connecting the metal ion and the M3H proton form an angle of about 90°. This very nicely explains the negative and smaller paramagnetic shift observed for the resonance of the mannose proton. It is noted in passing that in these qualitative considerations we have, for the sake of simplicity, assumed that we only need to deal with pseudocontact interactions. These are proportional to $(3\cos^2\theta - 1)/r^3$, where θ is the angle between the main principal axis of the paramagnetic susceptibility tensor and the axis connecting the metal ion and the proton considered; r is the distance between these two atoms. A further analysis of the conformation of BLM-Zn(II) in relation to the paramagnetic BLM-Fe(II) complex is outside the scope of this paper and would require more in-depth studies of the latter complex. It can be concluded, however, on the basis of the presently available data that the structures of the BLM-Zn(II) and BLM-Fe(II) complexes are similar, as has usually been assumed.

Biological Aspects. It is generally accepted that cell killing by bleomycin takes place via the DNA degradation of BLM-Fe(II)-O_2 complexes. The earlier research discussed above and the work carried out on other complexes of BLM analogues have suggested that the primary amine of the β-aminoalanine residue is a determinant in this biological activity, while the carbohydrate moiety and its attendant carbamoyl group is not. To an important extent these notions are based on ESR experiments carried out on different BLM congeners. On this basis, the BLM-Fe(II)-O_2 complex [and by interference the BLM-Fe(II)-CO complex] was assigned an octahedral coordination geometry with the primary amine function as an axial ligand. The secondary amine, the pyrimidine N_5, the deprotonated histidine amide, and the imidazole N_1 form the basal plane of the octahedron with a 5-5-6 chelate ring arrangement. The O_2 (or CO) is placed in an apical position with respect to the primary amine function, thus excluding the mannose carbamoyl group from metal coordination. This representation can be viewed as an extrapolation of the Cu(II)-P-3A complex, an abortive BLM congener, which lacks the carbohydrate residues and the bithiazole tail. As has already been indicated in the preceding section, exclusion of the carbamoyl group as a

(40) Sugiura, Y. *J. Am. Chem. Soc.* **1980**, *102*, 5208.
(41) Sugiura, Y.; Suzuki, T.; Muraoka, Y.; Umezawa, Y.; Takita, T.; Umezawa, H. *J. Antibiot.* **1981**, *43*, 1232.
(42) Sugiura, Y.; Suzuki, T.; Otsuma, M.; Kobayashi, S.; Ohno, M.; Takita, T.; Umezawa, H. *J. Biol. Chem.* **1983**, *258*, 1328.
(43) Sugiura, Y. *Biochem. Biophys. Res. Commun.* **1979**, *88*, 913.
(44) Oppenheimer, N. J.; Chang, C.; Chang, L.-H.; Ehrenfeld, G.; Rodriguez, L. O.; Hecht, S. M. *J. Biol. Chem.* **1982**, *257*, 1606.
(45) Pillai, R. P.; Lenkinski, R. E.; Sakai, T. T.; Geckle, J. H.; Krishna, N. R.; Glickson, J. D. *Biochem. Biophys. Res. Commun.* **1980**, *96*, 341.
(46) Crippen, G. M.; Oppenheimer, N. J.; Connolly, M. L. *Int. J. Pept. Protein Res.* **1981**, *17*, 156.
(47) Oppenheimer, N. J.; Rodriguez, L. O.; Hecht, S. M. *Biochemistry* **1979**, *18*, 3439.

ligand has been based on the similarity of the ESR parameters of different BLM congeners, i.e., metal complexes of BLM, iso-BLM, and deglyco-BLM.[41] On the other hand, the ESR parameters of dep-BLM are markably different.[40] This BLM congener is missing the alanine moiety and therefore its proposed axial ligand, the primary amine. The iron complex of a related analogue, the deamido-BLM, exhibits ESR parameters that are pH dependent,[40] i.e., at pH = 9 they are close to those of BLM–Fe(II)–NO, which has the same structure as BLM–Fe(II)–O_2, while at pH = 6 they are similar to those of the dep-BLM complex. The deamido-BLM complex has in its aminoalanine tail a carboxyl group replacing the primary amide such that it is thought that at pH = 6 the carboxyl group is coordinated to the iron ion, while at pH = 9 this is the primary amine. At pH = 6 the complex is not active just as the dep-BLM, but at pH = 9 it becomes active, suggesting a special role for the primary amine in the axial position.

The inability of the dep-BLM complex and of the deamido-BLM complex (at pH = 6) to produce nucleotide radicals from intact DNA[43,48] has been explained in terms of a deficient redox capacity of the corresponding oxygen adducts. Thus, in the native BLM–Fe(II)–O_2 complex, the proposed axially coordinated amine function is thought to play a crucial, if not decisive, role in the generation of the redox capacity and exclusion of the primary amine from metal coordination would lead to inactive complexes. Therefore, the conformation derived in this paper for the BLM–Fe(II)–CO complex would seem to be at variance with these ideas.

The ESR results need not, however, be explained in these terms. A case in point is the *N*-acetyl-BLM–Fe(II) complex, in which the primary amine group is acetylated and for which there are good reasons to assume that the primary amine group does not bind to the metal ion.[49] This BLM congener has indeed lost the ability to cleave DNA, but the reason is its inability to form a complex with oxygen (or CO) ligands. Comparison of the NMR spectra of the paramagnetic BLM–Fe(II) and *N*-acetyl-BLM–Fe(II) complexes shows that the coordination geometry of these two congeners is significantly different. Thus, the functional deficiency might well be caused by the abolishment of oxygen affinity in other cases as well, e.g., the behavior of the dep-BLM complex.

In our opinion it is too early to connect BLM functioning or disfunctioning, i.e., its DNA cleavage activity, with one particular group in the molecule. Scrutiny of the literature shows that modifications of the BLM molecule most times, if not always, lead to changes in the coordination geometry of the secondary and ternary complexes. In those cases where the β-aminoalanine portion of the molecule has been modified, it follows from ESR as well as NMR experiments that significant changes in coordination geometry take place.[40,49] When modifications of the carbohydrate moiety are effected, the ESR parameters are hardly influenced[41] but NMR experiments show that the coordination geometry has also changed in this case.[44] These changes in structure may influence BLM activity in several ways. As has been indicated, the oxygen affinity of the complex may be altered, but also an influence on the redox activity of the metal ion may not be ruled out. Furthermore, complex formation with DNA may be affected.

An example of the altered oxygen affinity has already been mentioned. Deglyco-BLM may perhaps serve as an example of the possible influence of modifications on DNA binding. It turns out that the redox activity of the deglyco-BLM is reduced, i.e., measured through the generation of [^{3}H]thymine from radiolabeled PM-2 DNA, which is reduced to about half of that obtained by the native BLM complex.[44] In addition to this reduced activity, the cleavage specificity of the deglyco-BLM is different from the normal BLM.[50,51] Thus, the sugar residues do influence the mechanism of cleavage. The present NMR results show that for normal BLM complexes the coordination of the carbamoyl group should be taken into account.

It is well-known from protein chemistry that in discussions about structure–function relationships the question often arises whether changes in activity can be assigned to just one residue or to more global properties of the molecule. With respect to the activity of BLM we face the same problem and therefore detailed structural studies, as the one performed in this paper, are necessary for modified BLM complexes.

Acknowledgment. This work was supported by the Dutch National Cancer Society, Koningin Wilhelmina Fonds (KWF). Spectra were recorded at the Dutch National NMR Facility (Nijmegen, The Netherlands) supported by Stichting Scheikundig Onderzoek Nederland (SON) and at Bruker Analytische Messtechnik GmbH (Rheinstetten, West Germany). We wish to thank Ing. J. v. Os and Ing. J. Joordens for technical assistance. Prof. I. D. Kuntz, of the Univeristy of California, is gratefully acknowledged for kindly providing (through Dr. C. A. G. Haasnoot) the distance geometry program. We also wish to thank the Dutch National CAOS/CAMM Facility at Nijmegen (The Netherlands) for assisting the Cambridge Crystallographic Data Base search.

(48) Sugiura, Y.; Muraoka, Y.; Fujii, A.; Takita, T.; Umezawa, H. *J. Antibiot.* **1979**, *32*, 756.

(49) Oppenheimer, N. J.; Rodriguez, L. O.; Hecht, S. M. *Biochemistry* **1980**, *19*, 4096.

(50) Sugiyama, H.; Kilkuskie, R. E.; Chang, L.-H.; Ma, L. T.; Hecht, S. M.; van der Marel, G. A.; van Boom, J. H. *J. Am. Chem. Soc.* **1986**, *108*, 3852.

(51) Sugiyama, H.; Kilkuskie, R. E.; Hechi, S. M.; van der Marel, G. A.; van Boom, J. H. *J. Am. Chem. Soc.* **1985**, *107*, 5983.